

Early Anomaly Detection and Location in Distribution Networks: A Data-Driven Approach

Xin Shi¹, *Member, IEEE*, Robert Qiu^{1,2}, *Fellow, IEEE*, Xing He¹, Zenan Ling¹, Haosen Yang¹, Lei Chu¹

Abstract—The online monitoring data in distribution networks contain rich information on the operating states of the networks. In this paper, by leveraging the data, a random matrix theory (RMT) based approach is proposed for early anomaly detection and location in distribution networks. First, a spatio-temporal matrix for each feeder line in the distribution network is formulated. Based on the Marchenko-Pastur Law for the empirical spectral analysis of covariance ‘signal+noise’ matrix, the linear eigenvalue statistics are introduced to indicate the anomaly, and the outliers and their corresponding eigenvectors are analyzed for locating the anomaly. As for the low observability feeders in the distribution network, an increasing data dimension algorithm is designed for the formulated low-dimensional matrices being more accurately analyzed. The proposed approach is capable of detecting and locating the early anomaly and robust against random fluctuations and measuring errors. Case studies on both synthetic data from IEEE standard bus systems and real-world online monitoring data in a distribution network corroborate the feasibility and effectiveness of the proposed approach.

Index Terms—early anomaly detection and location, distribution network, online monitoring data, random matrix theory, increasing data dimension

I. INTRODUCTION

THE distribution network is an important part of the power system, and its operating state is directly related to the safety of the entire system. One main factor that influences the operating state of the distribution network are the anomalies caused by overload, unbalanced three-phase voltage or current, system swing, etc. It is important for the safety analysis and decision making of control strategy to detect and locate the anomalies before power failures or system blackout. With numerous branch lines and complicated network topology, it becomes difficult to realize early anomaly detection and location in a distribution network. Furthermore, the anomalies may present intermittent, asymmetric, and sporadic spikes, which are random in magnitude and could involve sporadic bursts as well, and exhibit complex, nonlinear, and dynamic characteristics [1]. On this occasion, model-based methods are questionable because they are usually based on certain assumptions and simplifications.

This work was partly supported by National Key R & D Program of No. 2018YFF0214705, NSF of China No. 61571296 and (US) NSF Grant No. CNS-1619250.

¹ Department of Electrical Engineering, Center for Big Data and Artificial Intelligence, State Energy Smart Grid Research and Development Center, Shanghai Jiaotong University, Shanghai 200240, China. (e-mail: dugushixin@sjtu.edu.cn; rcqiu@sjtu.edu.cn; hexing_hx@126.com; ling_zenan@163.com; 2457604987@qq.com; leochu@sjtu.edu.cn;)

² Department of Electrical and Computer Engineering, Tennessee Technological University, Cookeville, TN 38505, USA. (e-mail:rcqiu@tntech.edu)

Along the years, there have been significant deployments of online monitoring devices in power systems, which lies the foundation to enable a true monitoring, such as linear state estimation [2], dynamic state estimator [3] or fully measurements of all state variables [4]. The massive data collected through them contain rich information on the operating states of the system, which stimulates the research on data analytics for anomaly detection and location. For example, in [5], one-class support vector machines (SVMs) is proposed for time-series novelty detection. In [6], the dimensionality of the phasor-measurement-unit (PMU) data is analyzed, and a PCA-based data dimensionality reduction algorithm is proposed for early event detection. In [7], stacked long short term memory (LSTM) networks are developed for time-series anomaly detection. In [8], by using massive streaming PMU data, a real-time anomaly detection algorithm based on multiple high-dimensional covariance matrix test is developed. In [9], a real-time anomaly detection and abnormal line identification approach is developed, which merges the early anomaly detection and location functionalities. In [10], a density-based detection algorithm is proposed to detect local outliers, which can differentiate high-quality synchrophasor data from the low-quality one during system physical disturbance. In [11], structured neural networks are proposed for anomaly detection in manufacturing systems.

Due to the massive data collected in a distribution network, the demand for theories capable of processing high-dimensional data has grown dramatically. The random matrix theory (RMT), introduced by Wishart in 1928 [12], is an important mathematical tool for statistical analysis of high-dimensional data. As for high-dimensional random matrices, the importance of the RMT for statistics comes from the fact that it may be used to correct traditional tests or estimators which fail in the ‘large p , large n ’ setting, where p is the number of parameters (dimensions) and n is the sample size. The RMT starts with asymptotic theorems on the distribution of eigenvalues or singular values of random matrices with certain assumptions, and eventually gives macroscopic quantity to indicate the data behavior. The theorems ensure convergence of the empirical eigenvalue distributions to deterministic functions as the matrices grow large, which makes the RMT naturally suitable for high-dimensional data analysis. Nowadays, the RMT has been widely used in wireless communication [13], finance [14], quantum information [15], etc. In recent years, some work that makes substantial use of results in the RMT has emerged in the power field. For example, in [16], an architecture with the application of the RMT into smart grid is proposed. In [17], based on the RMT, a

data-driven approach to reveal the correlations between various factors and the power system status is proposed. In [18] and [19], the RMT is used for power system transient analysis and steady-state analysis, respectively.

In this paper, based on the RMT, a data-driven approach is proposed for early anomaly detection and location in distribution networks. It leverages the similarities of the data amongst multiple monitoring devices, and realizes anomaly detection and location by tracking the variation of the data correlation. The main contribution of this paper can be summarized as follows: 1) The approach is purely data-driven and it only requires the simple topology information of feeder lines in the distribution network. 2) The approach merges anomaly detection and location functionalities by analyzing the extreme eigenvalues (outliers) and the corresponding eigenvectors from the data. 3) The approach is sensitive to the variation of the data correlation, which makes it possible for detecting the anomalies in an early phase. 4) It is experimentally justified that the approach is robust against random fluctuations and measuring errors of the data. 5) An increasing data dimension algorithm is designed, which makes it more accurate for analyzing the low observability feeder lines in the distribution network. 6) The proposed approach is suitable for both online and offline analysis.

The rest of this paper is organized as follows. Section II presents the mathematical foundations of RMT for anomaly detection and location, in which anomaly indicators are designed and analyzed. In section III, spatio-temporal matrices are formulated by using the online monitoring data in distribution networks and specific steps of the early anomaly detection and location approach are given. Meanwhile, an increasing data dimension algorithm is designed for analyzing the low observability feeders more accurately. Both synthetic data from IEEE standard bus system and real-world online monitoring data in a distribution network are used to validate the effectiveness of the proposed approach in section IV. Conclusions and future research directions are presented in Section V.

II. RANDOM MATRIX THEORY FOR ANOMALY DETECTION AND LOCATION

In practical world, massive amounts of data can be naturally represented by large random matrices [20]. In this section, we apply the RMT for anomaly detection and location of high-dimensional data matrices. First, asymptotic theorem in the RMT is used to analyze the empirical spectral distribution (ESD) of high-dimensional ‘signal+noise’ matrix, and linear statistics of the eigenvalues are introduced as a statistical index to track the data behavior. The details of the RMT for anomaly detection and location are given.

A. Asymptotic Theorem for ‘Signal+Noise’ Matrix

Marchenko-Pastur Law (M-P Law): Let $\mathbf{X} = \{x_{i,j}\}$ be a $p \times n$ random matrix, whose entries are independent identically distributed (i.i.d.) variables with the mean $\mu(x) = 0$ and the variance $\sigma^2(x) < \infty$. The corresponding covariance matrix is defined as $\Sigma = \frac{1}{n} \mathbf{X} \mathbf{X}^H$. As $p, n \rightarrow \infty$ but $c = \frac{p}{n} \in (0, 1]$,

according to the M-P law [21], the empirical spectral density of the Wishart matrix Σ converges to the limit with probability density function (PDF)

$$f_{MP}(x) = \begin{cases} \frac{1}{2\pi c \sigma^2 x} \sqrt{(b-x)(x-a)}, & a \leq x \leq b \\ 0, & \text{others} \end{cases}, \quad (1)$$

where $a = \sigma^2(1 - \sqrt{c})^2$, $b = \sigma^2(1 + \sqrt{c})^2$.

We apply the Marchenko-Pastur (M-P) law [21] for a high-dimensional data matrix $\mathbf{X}' \in \mathbb{R}^{p \times n}$. In normal state, \mathbf{X}' is considered to be a random matrix and the ESD of $\Sigma' = \frac{1}{n} \mathbf{X}' \mathbf{X}'^T$ converges to the limiting spectral density $f_{MP}(x')$, which is shown in Figure 1(a). The bars in blue color represent the eigenvalue distributions of Σ' and the M-P law is plotted in the red curve. However, what will happen in abnormal state? Here, ‘‘abnormal’’ means signals occur in \mathbf{X}' and the correlations among the entries x'_{ij} have been changed. Then \mathbf{X}' is considered of the type $\mathbf{X} + \mathbf{P}$, where \mathbf{X} is a random matrix which represents random noise or fluctuations, and \mathbf{P} is a low-rank matrix which represents anomaly signals. Figure 1(b) shows the ESD of Σ' can not be fit by the M-P law. It can be observed that the extreme eigenvalues (outliers) caused by anomaly signals are out of the range $[a, b]$ (i.e., $[0.034, 3.301]$).

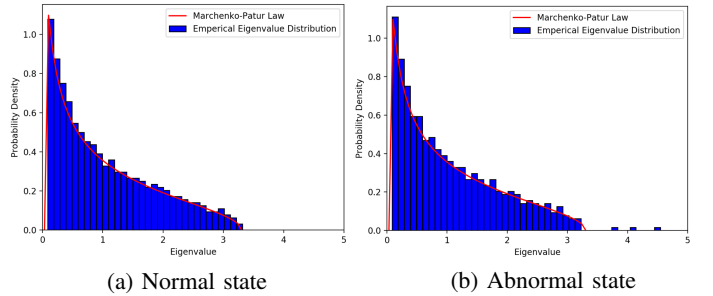


Fig. 1. The ESD of Σ' and its comparison with the theoretical M-P law under both normal and abnormal system states. (a) \mathbf{X}' is a 640×960 random gaussian matrix. (b) $\mathbf{X}' = \mathbf{X} + \mathbf{P}$, where \mathbf{X} is a 640×960 random gaussian matrix, and \mathbf{P} is a low-rank signal matrix.

Based on the analysis above, it can be concluded that the ESDs are different for a high-dimensional random matrix with or without anomaly signals, which inspires us to investigate the statistics regarding the empirical eigenvalues to indicate the data behavior. The linear eigenvalue statistics (LES) via test function ϕ are defined as

$$\mathcal{N}_\phi = \sum_{i=1}^n \phi(\lambda_i), \quad (2)$$

where $\lambda_i (i = 1, 2, \dots, n)$ are the eigenvalues, and the test function ϕ is smooth. The commonly used test functions include [20]:

- Chebyshev Polynomial (CP): $\phi(\lambda) = a_0 \lambda^n + a_1 \lambda^{n-1} + \dots + a_n$, where $a_i (i = 1, 2, \dots, n)$ are real numbers;
- Information Entropy (IE): $\phi(\lambda) = -\lambda \log \lambda$;
- Likelihood Ratio Function (LRF): $\phi(\lambda) = \lambda - \log \lambda - 1$;
- Wasserstein Distance (WD): $\phi(\lambda) = \lambda - 2\sqrt{\lambda} + 1$.

The LES constructed via the listed test functions does not introduce any system error, which can be served as an statistical index to track the data behavior. It gives insight into

the data behavior from a high-dimensional perspective, which makes it possible for detecting the latent anomalies in the data. Meanwhile, some statistical properties of the LES have been proved in theory [22], such as satisfying the central limit theorem, with bounded variance, with a fast decay rate (i.e., in the order of $O(p^{-2})$) for the variance, etc.

B. RMT for Anomaly Detection and Location

Assume there are P -dimensional measurement variables $(x_1, x_2, \dots, x_P) \in \mathbb{R}^P$ for each sampling time. At the sampling time t_j , the P -dimensional measurements can be formulated as a column vector $\mathbf{x}(t_j) = (x_1, x_2, \dots, x_P)^T$. For a series of time N , a data set \mathbf{D} is formulated by arranging these vectors \mathbf{x} in chronological order. Let \mathbf{X} be a $p \times n$ moving window on \mathbf{D} , we can convert it into the standard form $\hat{\mathbf{X}}$ by

$$\hat{x}_{ij} = (x_{ij} - \mu(\mathbf{x}_i)) \times \frac{\sigma(\hat{\mathbf{x}}_i)}{\sigma(\mathbf{x}_i)} + \mu(\hat{\mathbf{x}}_i), \quad (3)$$

where $\mathbf{x}_i = (x_{i1}, x_{i2}, \dots, x_{in})$, $\mu(\hat{\mathbf{x}}_i) = 0$, and $\sigma(\hat{\mathbf{x}}_i) = 1$ ($i = 1, 2, \dots, p; j = 1, 2, \dots, n$). The covariance matrix of $\hat{\mathbf{X}}$ is calculated as $\Sigma = \frac{1}{n} \hat{\mathbf{X}} \hat{\mathbf{X}}^T$. Then the empirical eigenvalues λ_Σ and eigenvectors \mathbf{v}_Σ of Σ can be obtained.

The linear statistics of λ_Σ is calculated through equation (2), which is served as the anomaly detection indicator in the proposed approach. Furthermore, the anomaly is located based on the calculated λ_Σ and \mathbf{v}_Σ . According to the matrix theory, we can obtain

$$\Sigma \mathbf{v}_{\Sigma,k} = \lambda_{\Sigma,k} \mathbf{v}_{\Sigma,k}. \quad (4)$$

The derivation of equation (4) regarding the elements ε_{ij} is

$$\frac{d\Sigma}{d\varepsilon_{ij}} \mathbf{v}_{\Sigma,k} + \Sigma \frac{d\mathbf{v}_{\Sigma,k}}{d\varepsilon_{ij}} = \frac{d\lambda_{\Sigma,k}}{d\varepsilon_{ij}} \mathbf{v}_{\Sigma,k} + \lambda_{\Sigma,k} \frac{d\mathbf{v}_{\Sigma,k}}{d\varepsilon_{ij}}. \quad (5)$$

Since Σ is real and symmetric, and there exist $\mathbf{v}_{\Sigma,k}^T \mathbf{v}_{\Sigma,k} = 1$. Left multiply $\mathbf{v}_{\Sigma,k}^T$ for equation (5), we can obtain

$$\frac{d\lambda_{\Sigma,k}}{d\varepsilon_{ij}} = \mathbf{v}_{\Sigma,k}^T \frac{d\Sigma}{d\varepsilon_{ij}} \mathbf{v}_{\Sigma,k}, \quad (6)$$

where $\frac{d\Sigma}{d\varepsilon_{ij}}$ gets the value of 1 only for the entry ε_{ij} in Σ and 0 for others. Thus the equation (6) can be simplified as

$$\frac{d\lambda_{\Sigma,k}}{d\varepsilon_{ij}} = v_{\Sigma,k}^{(i)} v_{\Sigma,k}^{(j)}. \quad (7)$$

Then the contribution of the i -th row's elements to $\lambda_{\Sigma,k}$ can be measured by

$$\sum_{j=1}^p \left(\frac{d\lambda_{\Sigma,k}}{d\varepsilon_{ij}} \right)^2 = (v_{\Sigma,k}^{(i)})^2 \sum_{j=1}^p (v_{\Sigma,k}^{(j)})^2 = (v_{\Sigma,k}^{(i)})^2. \quad (8)$$

From equation (8), it can be concluded that the contribution rate of the i -th ($1 \leq i \leq p$) row to the eigenvalue $\lambda_{\Sigma,k}$ of the covariance matrix Σ can be measured by the i -th element of the corresponding eigenvector $\mathbf{v}_{\Sigma,k}$. Based on the analysis of the M-P law for high-dimensional 'signal+noise' matrix in Section II-A, it can be observed that outliers (i.e., $\lambda > b$) occur when a system operates in abnormal state. This inspires us to realize anomaly location by studying the

eigenvectors corresponding to the outliers. Here, an anomaly location indicator is designed as

$$\eta_i = \frac{\sum_{\lambda_{\Sigma,k} \in \{\lambda > b\}} \lambda_{\Sigma,k} (v_{\Sigma,k}^{(i)})^2}{\sum \lambda_{\Sigma,k}}, \quad (9)$$

where $\eta_i \in [0, 1)$. The indicator η_i measures the scale of the i -th row's contribution to the anomaly.

We first standardize $\boldsymbol{\eta}$ ($\eta_i \in \boldsymbol{\eta}$) by

$$\hat{\boldsymbol{\eta}} = \frac{\boldsymbol{\eta} - \mu(\boldsymbol{\eta})}{\sigma(\boldsymbol{\eta})}, \quad (10)$$

where $\mu(\boldsymbol{\eta})$ and $\sigma(\boldsymbol{\eta})$ are the mean and standard deviation of $\boldsymbol{\eta}$, and $\hat{\boldsymbol{\eta}}$ ($\hat{\eta}_i \in \hat{\boldsymbol{\eta}}$) is the standard form of $\boldsymbol{\eta}$. Considering the sample size p of $\hat{\boldsymbol{\eta}}$ is sometimes small, here, $\hat{\boldsymbol{\eta}}$ is considered to follow the student's t-distribution with $p - 1$ degrees of freedom. According to the central limit theorem, the confidence level $1 - \alpha$ for the population mean μ of $\hat{\boldsymbol{\eta}}$ is defined as

$$1 - \alpha = P\left\{ \mu(\hat{\boldsymbol{\eta}}) - t_{\frac{\alpha}{2}} \frac{\sigma(\hat{\boldsymbol{\eta}})}{\sqrt{p}} < \mu < \mu(\hat{\boldsymbol{\eta}}) + t_{\frac{\alpha}{2}} \frac{\sigma(\hat{\boldsymbol{\eta}})}{\sqrt{p}} \right\}, \quad (11)$$

where $\mu(\hat{\boldsymbol{\eta}})$ and $\sigma(\hat{\boldsymbol{\eta}})$ are the sample mean and standard deviation of $\hat{\boldsymbol{\eta}}$ with $\mu(\hat{\boldsymbol{\eta}}) = 0$ and $\sigma(\hat{\boldsymbol{\eta}}) = 1$, $t_{\frac{\alpha}{2}}$ is the upper $\frac{\alpha}{2}$ critical value for the t distribution with $p - 1$ degrees of freedom, and $P\{\cdot\}$ is the probability operator. For a given $\hat{\eta}_i$, the corresponding confidence level $1 - \alpha$ can be obtained by the t distribution table. For example, let $\hat{\eta}_i = 2.650$ and $p = 14$, then the confidence level $1 - \alpha$ is 98%. Thus, the anomaly location can be determined by comparing $1 - \alpha$ with $(1 - \alpha)_{th}$.

In real-time analysis, we can move the window at continuous sampling times and the last sampling time is the current time, which enables us to track the data behavior effectively. For example, at the sampling time t_j , the obtained data matrix $\mathbf{X}(t_j)$ is formulated as

$$\mathbf{X}(t_j) = (\mathbf{x}(t_{j-n+1}), \mathbf{x}(t_{j-n+2}), \dots, \mathbf{x}(t_j)), \quad (12)$$

where $\mathbf{x}(t_k) = (x_1, x_2, \dots, x_p)^T$ for $t_{j-n+1} \leq t_k \leq t_j$ is the sampling data at time t_k . Thus, $\mathcal{N}_\phi(t_j)$ and $\boldsymbol{\eta}(t_j)$ are produced for the sampling time t_j .

III. EARLY ANOMALY DETECTION AND LOCATION IN DISTRIBUTION NETWORKS

In this section, by leveraging the online monitoring data in distribution networks, the RMT-based early anomaly detection and location approach is proposed. First, the online monitoring data for each feeder line is formulated as a spatio-temporal data set. Then, steps of the proposed approach are provided, and the advantages of it are systematically analyzed. Last, an increasing data dimension algorithm is designed for the low observability feeders being more accurately analyzed.

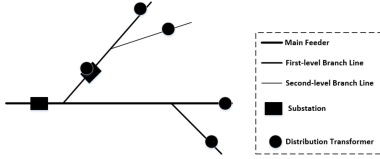


Fig. 2. Circuitry topology diagram of partial distribution network.

A. Formulation of Online Monitoring Data as Spatio-Temporal Matrices

Figure 2 illustrates circuitry topology diagram of partial distribution network, in which a feeder line consists of different level of branch lines and substations with distribution transformers. Multiple online monitoring devices are installed at different physical locations of the feeder, through which we can obtain many types of measurement variables, such as three-phase voltage (u_a, u_b, u_c) , three-phase current (i_a, i_b, i_c) , active load (l) , etc. Here, 7 measurements $(u_a, u_b, u_c, i_a, i_b, i_c, l)$ at the sampling time t_j are chosen as the elements to formulate a data vector $\mathbf{d}(t_j) = [u_{aj}^{(1)}, u_{bj}^{(1)}, u_{cj}^{(1)}, i_{aj}^{(1)}, i_{bj}^{(1)}, i_{cj}^{(1)}, l_j^{(1)}, \dots, l_j^{(m)}]^T$, where m denotes the number of monitoring devices installed on the feeder line. Assume $P = 7m$, for a series of time N , we can obtain the data set $\mathbf{D} = [\mathbf{d}(t_1), \mathbf{d}(t_2), \dots, \mathbf{d}(t_N)] \in \mathbb{R}^{P \times N}$. It is noted that, by stacking the measurements together, the formulated spatio-temporal data set contains rich information on the operating state of the feeder line.

B. early anomaly Detection and Location Approach

Based on the research mentioned above, an early anomaly detection and location approach in distribution networks is proposed. The specific steps are given in Table III-B.

Steps of the RMT for early anomaly Detection and Location in Distribution Networks

- 1: For each feeder, a spatio-temporal data set $\mathbf{D} \in \mathbb{R}^{P \times N}$ is formulated by arranging P measurements in a series of time N .
- 2: At each sampling time t_j :
 - 2a) Obtain the data matrix $\mathbf{X}(t_j)$ by using a $p \times n$ ($p = P, n < N$) window on \mathbf{D} ;
 - 2b) Convert $\mathbf{X}(t_j)$ into the standard form matrix $\hat{\mathbf{X}}(t_j)$ through equation (3);
 - 2c) Calculate the sample covariance matrix of $\hat{\mathbf{X}}(t_j)$, i.e., $\Sigma(t_j)$;
 - 2d) Obtain the eigenvalues $\lambda_{\Sigma}(t_j)$ and eigenvectors $\mathbf{v}_{\Sigma}(t_j)$, and compare the ESD with the theoretical limits;
 - 2e) Calculate the linear statistics of $\lambda_{\Sigma}(t_j)$ through equation (2), i.e., $\mathcal{N}_{\phi}(t_j)$;
 - 2f) Calculate the location indicator $\eta(t_j)$ through equation (9).
- 3: Draw the $\mathcal{N}_{\phi} - t$ curve for each feeder in a series of time N .
- 4: Plot the 3D graph of η regarding the P measurements and time N , and calculate the confidence level $1 - \alpha$ corresponding to each data point to locate the anomaly indexes.

The early anomaly detection and location approach is driven by the online monitoring data in distribution networks, and based on the RMT. It is sensitive to the variation of the data correlation, which makes it possible for detecting the anomalies in an early phase. The steps above involve no mechanism models, thus avoiding the errors brought by assumptions and simplifications. The approach merges anomaly detection and

location functionalities, and experimentally robust against random fluctuations and measuring errors for the reason of large size data window. What's more, the proposed approach is practical for both online and offline analysis by using the moving window method.

C. More Discussions about the Proposed Approach

We may notice that the M-P law holds when the data dimensions are infinite or large. However, in the application of early anomaly detection and location in distribution networks, there exist some low observability feeders. Dimensions of the formulated data matrices corresponding to those feeders are often moderate, such as tens or less. In [23] and [24], a natural way of increasing dimensions of data vectors based on tensor product is introduced. On this basis, here, an algorithm to increase dimensions of data matrices is designed. The algorithm allows for the analysis of high-dimensional data matrices and yields smaller variance for the related functionals.

Assume $\mathbf{X} = [\mathbf{x}_1, \mathbf{x}_2, \dots, \mathbf{x}_t] \in \mathbb{C}^{p \times t}$ be a random matrix with i.i.d. entries, $p = kn$. For $k, t, n \in \mathbb{N}$, we construct a new random vector by using the tensor product of the column vectors of \mathbf{X} in the form

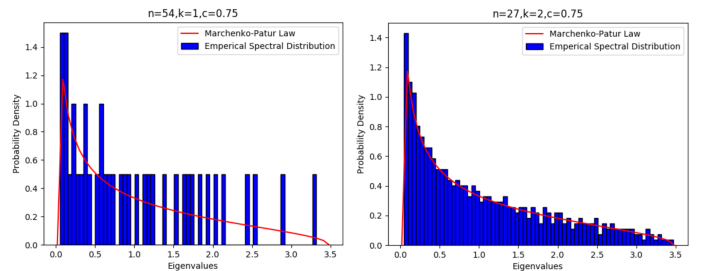
$$\tilde{\mathbf{x}}_j = \mathbf{x}_j^{(1)} \otimes \dots \otimes \mathbf{x}_j^{(k)} \in (\mathbb{C}^n)^{\otimes k}, \quad (13)$$

where $\mathbf{x}_j^{(l)}$ ($j = 1, 2, \dots, n; l = 1, 2, \dots, k$) are i.i.d. copies of a normalized isotropic random vector $\mathbf{x}_j^{(1)} = (x_{1j}, \dots, x_{nj}) \in \mathbb{C}^n$, and \otimes denotes the tensor product operation. The new random vector $\tilde{\mathbf{x}}_j$ lies in the n^k dimensional normed space. Thus, the corresponding dimension increased random matrix $\tilde{\mathbf{X}} = [\tilde{\mathbf{x}}_1, \tilde{\mathbf{x}}_2, \dots, \tilde{\mathbf{x}}_t] \in \mathbb{C}^{n^k \times t}$ is obtained. The time and space complexity of the algorithm are $O(kt)$ and $O(n^k)$.

Now consider $n^k \times n^k$ random matrices of the form

$$\mathcal{M}_{n,t,k}(\mathbf{x}) = \sum_{\alpha=1}^t \tau_{\alpha} \tilde{\mathbf{x}}_{\alpha} \tilde{\mathbf{x}}_{\alpha}^H, \quad (14)$$

where τ_{α} ($\alpha = 1, 2, \dots, t$) are real numbers. The asymptotic behavior of $\mathcal{M}_{n,t,k}(\mathbf{x})$ has been well studied in [25]. For every fixed $k \geq 1$, as $t \rightarrow \infty, n \rightarrow \infty$, but $\frac{t}{n^k} \rightarrow c \in (0, \infty)$, the ESD of $\mathcal{M}_{n,t,k}(\mathbf{x})$ converges to a non-random measure.



(a) Dimension: 54

(b) Dimension: 729

Fig. 3. The ESD of $\mathcal{M}_{n,t,k}(\mathbf{x})$ and its comparison with the M-P law. The dimension of \mathbf{X} is increased from $27 \times 2 = 54$ to $27^2 = 729$ through a tensor product of its column vectors, the ratio c is 0.75, and τ_{α} is 1.

The ESD of the original covariance random matrix and the tensor product version and their comparisons with the theoretical M-P law are plotted in Figure 3(a) and Figure 3(b),

TABLE I
ASSUMED SIGNAL FOR ACTIVE LOAD OF BUS 101 IN CASE 1.

Bus	Sampling Time	Active Load(MW)
101	$t_s = 1 \sim 500$	20
	$t_s = 501 \sim 1000$	100
Others	$t_s = 1 \sim 1000$	Unchanged

respectively. It can be observed that the ESD of the original covariance random matrix does not fit the M-P law for the reason of low dimensions. In contrast, the ESD of the tensor product version of covariance random matrix converges almost surely to the theoretical limits. The increasing data dimension algorithm makes it more accurate for analyzing the formulated low-dimensional data matrices from low observability feeders in the distribution network.

IV. CASE STUDIES

In this section, the effectiveness of the proposed approach is validated with both the synthetic data from the standard IEEE bus test system [26] and the real-world online monitoring data from a distribution network. Six cases in different scenarios are designed: 1) In the first four cases, by using the synthetic data, we validate the effectiveness of the proposed approach with different test functions, the designed increasing data dimension algorithm, the anomaly location function and the advantages of the proposed approach. 2) The last two cases, leveraging the real-world online monitoring data, validate the effectiveness of the proposed approach for both high and low observability feeders in the distribution network.

A. Case Study with Synthetic Data

The synthetic data was generated from IEEE 118-bus, 30-bus, 33-bus and 57-bus test systems [26]. See case118.m, case30.m, case33.m and case57.m in Matpower package [27] for details. For the generated data \mathbf{D} , a little noise \mathbf{E} was introduced to represent random fluctuations and measuring errors, i.e., $\mathbf{D} = \mathbf{D} + \gamma\mathbf{E}$. The scale of the added noise is $\gamma = \sqrt{\frac{Tr(\mathbf{D}\mathbf{D}^H)}{Tr(\mathbf{E}\mathbf{E}^H) \times \tau_{SNR}}}$, where $Tr(\cdot)$ represents the trace function and τ_{SNR} is the signal-to-noise ratio. In case 1 and case 2, the white noise was introduced, i.e., $E \sim N(0, 1)$; in case 3 and case 4, the colored noise was introduced, i.e., $E_{it} = 0.5 * E_{i,t-1} + \varepsilon_{it}$, where $\varepsilon_{it} \sim N(0, 1 - 0.5^2)$ so that the variance of E_t is 1.

1) Case Study on Different Test Functions: In this case, the synthetic data generated from IEEE 118-bus test system contained 118 voltage measurement variables with sampling 1000 times. In order to test the effectiveness of the proposed approach with different test functions in equation (2), an assumed anomaly signal was set by a sudden change of active load at bus 101 and others stayed unchanged, which was shown in Table I. The generated data was shown in Figure 4. In the experiment, the size of the moving window was set as 118×200 and τ_{SNR} was set to be 500.

The anomaly detection results of the proposed approach with different test functions are normalized into $[0, 1]$, which are shown in Figure 5. It is noted that the $\mathcal{N}_\phi - t$ curve begins

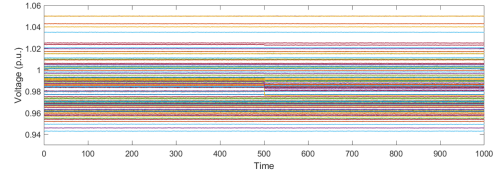


Fig. 4. The synthetic data generated from IEEE 118-bus test system in Case 1. One anomaly signal was set at $t_s = 501$.

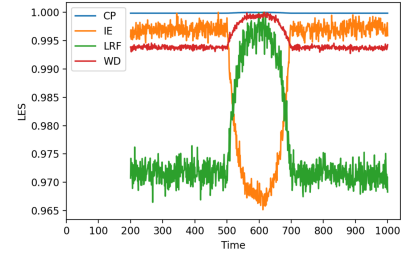


Fig. 5. Effectiveness of the proposed approach with different test functions.

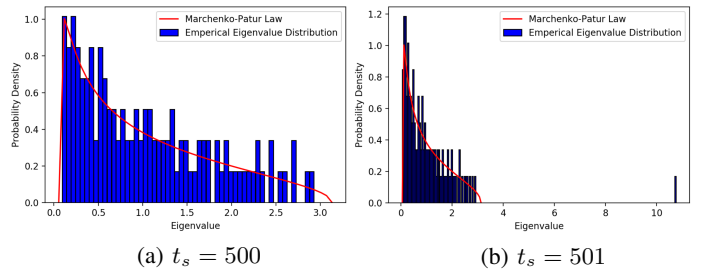


Fig. 6. The ESD and its comparison with theoretical M-P law in Case 1.

at $t_s = 200$, because the initial moving window includes 199 times of historical sampling and the present sampling data. From the $\mathcal{N}_\phi - t$ curves, it can be observed:

I. During $t_s = 200 \sim 500$, \mathcal{N}_ϕ computed through the proposed approach with 4 different test functions remain almost constant, which indicates the system operates in normal state. As is shown in Figure 6(a), the ESD converges almost surely to the theoretical M-P law.

II. From $t_s = 501$, \mathcal{N}_ϕ begin to change rapidly, which indicates anomaly signal occurs. Figure 6(b) shows that there exists one outlier, which coincide with the assumed anomaly signal in Table I. It is noted that, from $t_s = 501 \sim 700$, the $\mathcal{N}_\phi - t$ curves are almost U-shaped or inverted U-shaped, because the delay lag of the signal to \mathcal{N}_ϕ is equal to the moving window's width. What's more, the $\mathcal{N}_\phi - t$ curve corresponding to test function IE has the highest variance ratio, which indicates the anomaly indicator via test function IE is more sensitive to the anomaly data behavior. Hence IE was chosen as the test function in subsequent cases.

2) Case Study on Increasing Data Dimensions: In this case, the effectiveness of the designed increasing data dimension algorithm was tested. The synthetic data generated from IEEE 30-bus test system contained 30 voltage measurement variables with sampling 1000 times. In the simulation, an assumed anomaly signal was set by a sudden change of the active load at bus 20 and others stayed unchanged, which was shown in Table II. The generated data was shown in Figure 7. In the

TABLE II
ASSUMED SIGNAL FOR ACTIVE LOAD OF BUS 20 IN CASE 2.

Bus	Sampling Time	Active Load(MW)
20	$t_s = 1 \sim 500$	20
	$t_s = 501 \sim 1000$	30
Others	$t_s = 1 \sim 1000$	Unchanged

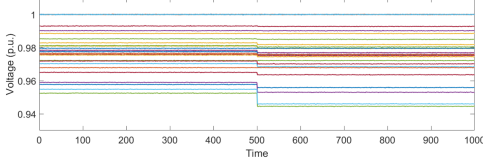


Fig. 7. The synthetic data generated from IEEE 30-bus test system in Case 2. One anomaly signal was set at $t_s = 501$.

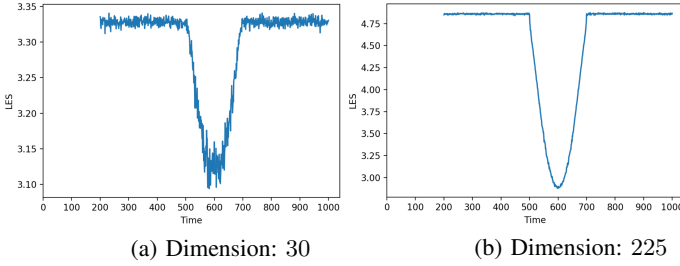


Fig. 8. The anomaly detection results corresponding to different data dimensions. The dimension of the data was increased from $30 = 15 \times 2$ to $225 = 15^2$.

experiment, the size of the moving window was 30×200 , the parameter τ_α in equation (14) was 1, and the signal-to-noise ratio τ_{SNR} defined in Case 1 was 500. By using the designed increasing data dimension algorithm, dimension of each data window was increased from $30 = 15 \times 2$ to $225 = 15^2$.

Figure 8(a) and 8(b) show the anomaly detection results corresponding to different data dimensions. From the $\mathcal{N}_\phi - t$ curves, it can be obtained:

I. During $t_s = 200 \sim 500$, the values of \mathcal{N}_ϕ remain almost at 3.33, 4.76, respectively, which indicates the system operates in normal state. The ESD does not fit the theoretical M-P law in Figure 9(a) for the reason of low data dimensions. In contrast, as shown in Figure 9(b), the ESD converges almost surely to the theoretical limits after increasing the data's dimension from 30 to 225.

II. From $t_s = 501$, the $\mathcal{N}_\phi - t$ curves begin to change rapidly, which indicates anomaly signal occurs and the system operates in abnormal state. For example, during $t_s = 501 \sim 600$, the values of \mathcal{N}_ϕ reduce almost from 3.32, 4.75 to 3.10, 2.80, respectively. The ESD does not fit the theoretical M-P law for the reason of existing outliers, which are shown in Figure 9(c) and 9(d). The difference lies that more outliers occur and the maximum outlier value becomes larger when the data dimension is increased from 15 to 225, which makes it much easier to detect the anomaly behavior of the data. What's more, the $\mathcal{N}_\phi - t$ curve corresponding to high data dimension is smoother, which indicates the designed increasing data dimension algorithm can help improve the robustness of the proposed approach against random fluctuations and measuring errors in the data.

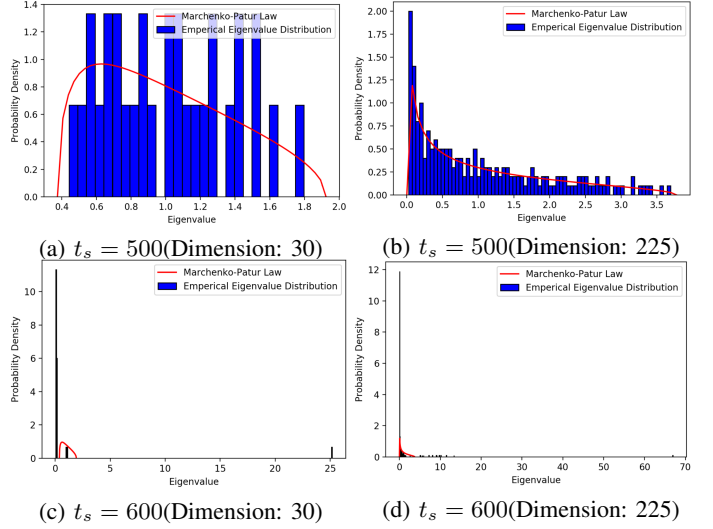


Fig. 9. The ESD and its comparison with theoretical M-P law in Case 2.

TABLE III
ASSUMED SIGNAL FROM BUS 21 TO 22 IN CASE 3.

fBus	tBus	Sampling Time	Impedance(p.u.)
21	22	$t_s = 1 \sim 500$	0.5
		$t_s = 501 \sim 1000$	20
Others	Others	$t_s = 1 \sim 1000$	Unchanged

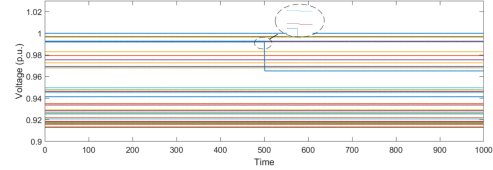


Fig. 10. The synthetic data generated from IEEE 33-bus distribution test system in Case 3. The anomaly indexes were 20 ~ 22.

3) Case Study On Anomaly Location: In this case, the proposed anomaly location approach was tested by using the synthetic data from IEEE 33-bus distribution test system. The data contained 33 voltage measurement variables with sampling 1000 times. In the simulation, an assumed anomaly signal was set by a sudden increase of impedance from bus 21 to 22 and others stayed unchanged, which was shown in Table III. The generated data with anomaly indexes labelled was shown in Figure 10. In the experiment, the size of the moving window was set as 33×200 , and the signal-to-noise ratio τ_{SNR} defined in Case 1 was 1000.

The anomaly location result is shown in Figure 11(a). It can be observed that, from $t_s = 501$, the location indicator $\eta_{20 \sim 22}$ increase rapidly and others stay almost unchanged, which indicates anomaly occurs on bus 20 ~ 22. For example, at $t_s = 501$, the calculated $1 - \alpha$ corresponding to bus 20 ~ 22 and others (such as bus 23) are 96.65%, 99.59%, 99.91%, and 24.38%, respectively. The anomaly location result coincides with the real anomaly indexes.

Furthermore, we explore the effectiveness of the proposed anomaly location approach when the data's dimension is increased from $33 = 16 + 17$ to $272 = 16 \times 17$. The anomaly location result is shown in Figure 11(b). It can

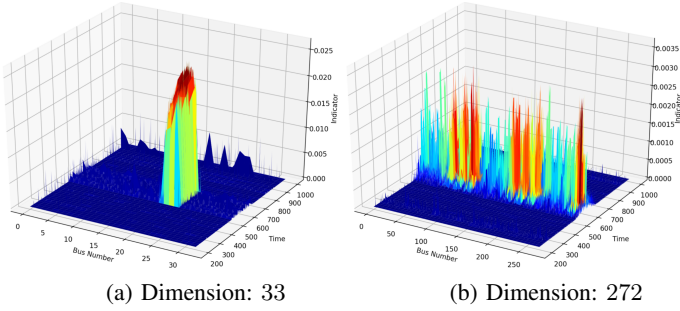


Fig. 11. The anomaly location results corresponding to different data dimensions. The dimension of the data was increased from 33 to 272.

TABLE IV
ASSUMED SIGNAL FOR ACTIVE LOAD OF BUS 20 IN CASE 4.

Bus	Sampling Time	Active Power(MW)
20	$t_s = 1 \sim 500$	10
20	$t_s = 501 \sim 1000$	10 \rightarrow 60
Others	$t_s = 1 \sim 1000$	Unchanged

be observed that, from $t_s = 501$, the location indicator $\eta_{3 \sim 5, 20 \sim 22, \dots, 258 \sim 260}$ increase rapidly and others stay almost unchanged. Let $\mathbf{I} = \{3 \sim 5, 20 \sim 22, \dots, 258 \sim 260\}$, at $t_s = 501$, the calculated $1 - \alpha$ corresponding to \mathbf{I} and others (such as 6) are $\{98.84\% \sim 99.50\%, 86.04\% \sim 87.35\%, \dots, 99.63\% \sim 99.77\%\}$ and 44.23%, respectively. Assume $n = 17$, the anomaly location in the original data matrix can be calculated by $\{(\mathbf{I} \bmod n) + n\}$, i.e., $\{20 \sim 22\}$, which coincides with the real anomaly indexes.

4) Case Study on Comparison with Other Approaches: In this case, we compare our spectrum analysis (SA) approach with SVMs [5], AEs [11] and LSTM [7] to illustrate the advantages of the proposed approach for anomaly detection, i.e., more sensitive to the variation of the data behavior and robust against random fluctuations and measuring errors. The IEEE 57-bus test system can be considered as a distribution test system connected with distributed generators, and it is used to generate the synthetic data. In the simulation, an increasing anomaly signal was set by a gradual increase of active load at bus 20 and others stayed unchanged, which was shown in Table IV. The generated data contained 57 voltage measurement variables with sampling 1000 times, which was shown in Figure 12. In the experiment, the signal-to-noise ratio τ_{SNR} was set as 1000. For SVMs, AEs and LSTM, we trained the detection models only using a normal data sequence during $t_s = 1 \sim 200$ and computed the testing errors for the remaining sequence during $t_s = 201 \sim 1000$, in which one time of sampling was used as a training/testing sample. For the proposed approach, both the approach itself (SA) and its combination with the designed increasing data dimension algorithm (SA+IDD) were tested. The parameters involved in the detection approaches are summarized as in Table V.

The anomaly detection results of different approaches are normalized into $[0, 1]$, which are shown in Figure 13. For SVMs, the normalization result of signed distance to the separating hyperplane is plotted; for AEs and LSTM, the normalized values of testing errors are plotted; for SA and SA+IDD, $1 - \hat{\mathcal{N}}(\phi)$ is plotted, where $\hat{\mathcal{N}}(\phi)$ is the normalized

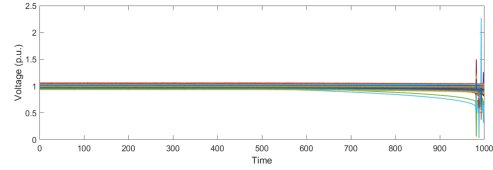


Fig. 12. The synthetic data generated from IEEE 57-bus test system. An increasing anomaly signal was set at $t_s = 501$. With the increase of the anomaly signal, the voltage collapses at $t_s = 980$.

TABLE V
PARAMETER SETTINGS INVOLVED IN THE DETECTION APPROACHES.

Approaches	Parameter Settings
SVMs	the upper bound on the fraction of training errors v : 0.03; the kernel function: $K(\mathbf{x}_i, \mathbf{x}_j) = (0.01\mathbf{x}_i^T \mathbf{x}_j)^3$; the model depth: 3; the number of neurons in each layer of encoder: 57, 32, 16;
AEs	the number of neurons in each layer of decoder: 16, 32, 57; the initial learning rate: 0.001; the activation function: <i>sigmoid</i> ; the minimum reconstruction error: 0.00001; the optimizer: <i>Adam</i> .
LSTM	the time steps: 1; the model depth: 3; the number of neurons in each layer: 57, 64, 57; the initial learning rate: 0.001; the activation function: <i>sigmoid, tanh</i> ; the minimum reconstruction error: 0.00001; the optimizer: <i>Adam</i> .
SA	the moving window's size: 57×200 ;
SA+IDD	the moving window's size: 57×200 ; the parameter τ_α : 1; the increased data dimension: $812 = 28 \times 29$.

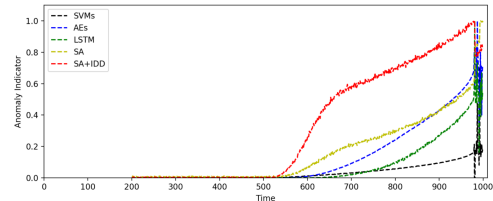


Fig. 13. The anomaly detection results of different approaches in Case 4.

form of $\hat{\mathcal{N}}_\phi$. It can be observed that, SA+IDD and SA are able to detect the anomaly signal much earlier (i.e., $t_s = 530 \sim 540$) than other approaches, which validates the proposed approach is more sensitive to the variation of the data behavior and robust against random fluctuations and measuring errors. The reason is that, in the proposed approach, a large size data window instead of just the current sampling data is analyzed for each sampling time. The average result makes the proposed approach more robust against random fluctuations and measuring errors of the data. Meanwhile, it is noted that SA+IDD outperforms SA in anomaly detection, which indicates the designed increasing data dimension algorithm can help improve the detection performance of SA approach.

Furthermore, in order to illustrate the efficiency of different detection approaches, the *average calculation time (ACT)* for each sampling time was counted. For SVMs, AEs and

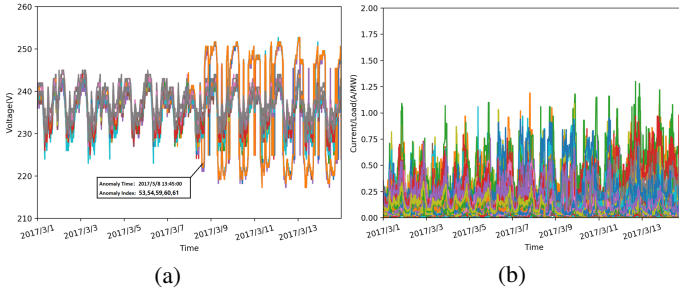


Fig. 14. The real-world online monitoring data with anomaly time and location recorded in Case 5. (a) Three-phase voltage magnitude curves. (b) Three-phase current and active load magnitude curves. The recorded anomaly time was 2017/3/8 13:45:00 and anomaly indexes were 53, 54, 59, 60, 61.

LSTM, the *ACT* for each testing sample was counted, which does not include the model training time. The experiments were conducted on a server with 2.60 GHz central processing unit (CPU) and 8.00 GB random access memory (RAM). The *ACT* for SVMs, AEs, LSTM, SA and SA+IDD are 0.001, 0.001, 0.002, 0.002 and 0.029 (unit: s), respectively. Considering the proposed approach is an unsupervised approach without any training, it can be concluded that the proposed approach has competitive performance in efficiency.

B. Case Study with Real-World Online Monitoring Data

The online monitoring data obtained from a real-world distribution network in Hangzhou city of China was used to test the effectiveness of the proposed approach. The distribution network contained 200 feeder lines with 8000 distribution transformers. For each feeder line, multiple online monitoring devices were installed in different physical locations and the data were sampled every 15 minutes. Anomaly information for each feeder line was recorded during the operation. In the following cases, three-phase voltage, three-phase current and active load sampled from March 1st, 2017 to March 14th, 2017 were chosen as the measurement variables to formulate the data matrices.

5) Case Study on High Observability Feeders: In this case, the proposed approach was validated by analyzing a high-dimensional online monitoring data set from one feeder line. The data collected from 17 monitoring devices installed on the feeder contained $17 \times 7 = 119$ measurement variables, thus a 119×1344 data set was formulated. The data with anomaly time and location recorded was shown in Figure 14. In the experiment, the size of the moving window was set as 119×192 . The generated $\mathcal{N}_\phi - t$ curve with continuously moving windows was shown in Figure 15(a). In the figure, the red dashed line marked the recorded anomaly time. The early anomaly detection process is shown as follows:

I. During 2017/3/3 00:00:00~2017/3/7 22:30:00, \mathcal{N}_ϕ remains almost constant, which indicates the feeder operates in normal state.

II. From 2017/3/7 22:30:00, \mathcal{N}_ϕ begins to decrease rapidly, which indicates early anomaly signals occur and the state of the feeder begins to deteriorate. Considering the recorded anomaly time is 2017/3/8 13:45:00, it can be concluded that the anomaly is detected in an early phase by the proposed

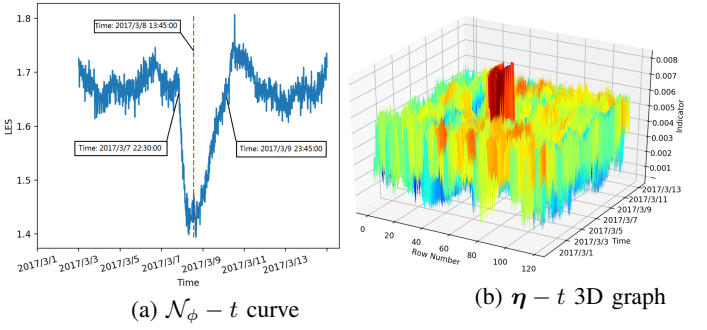


Fig. 15. Early anomaly detection and location for high-dimensional feeder.

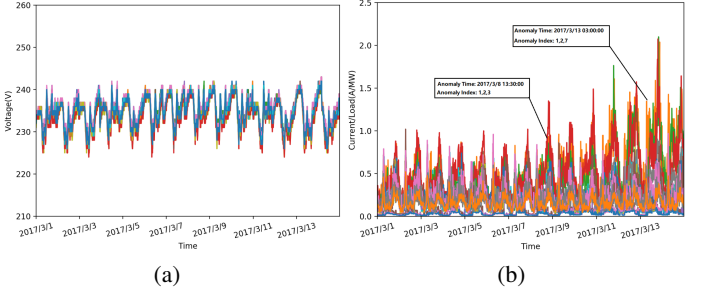


Fig. 16. The real-world online monitoring data with anomaly time and location recorded in Case 6. (a) Three-phase voltage magnitude curves. (b) Three-phase current and active load magnitude curves. The anomaly time and indexes were 2017/3/8 13:30:00, 2017/3/13 03:00:00 and $\{1, 2, 3\}$, $\{1, 2, 7\}$, respectively.

approach. Meanwhile, it is noted that, from 2017/3/7 22:30:00 to 2017/3/9 23:45:00, the $\mathcal{N}_\phi - t$ curve is almost U shaped and the delay lag of the anomaly signal to \mathcal{N}_ϕ is equal to the moving window's width, which coincides with our simulation result in Case 1.

Figure 15(b) is the 3D plot of location indicator η regarding 119 measurement variables from 2017/3/3 00:00:00 to 2017/3/14 23:45:00. It can be observed that, from 2017/3/7 22:30:00, $\eta_{\{53,54,59,60,61\}}$ increase rapidly and they are larger than others (such as η_{100}), thus we can determine the anomaly index $\mathbf{I} = \{53, 54, 59, 60, 61\}$. For example, at 2017/3/7 22:45:00, the calculated values of $1 - \alpha$ corresponding to $\eta_{\mathbf{I}}$ and η_{100} are 99.89%, 99.91%, 99.92%, 99.91%, 99.93% and 34.65%, respectively. The anomaly location result coincides with the recorded indexes.

6) Case Study on Low Observability Feeders: In this case, the combination of the designed increasing data dimension algorithm and the proposed approach was verified by using a low-dimensional online monitoring data set from one low observability feeder line. The data collected from 6 monitoring devices contained $6 \times 7 = 42$ monitoring measurements, thus a 42×1344 data set was formulated. The low-dimensional data with anomaly time and location labelled was shown in Figure 16. In the experiment, the size of the moving window was set as 42×196 . For each moving window, the dimension was increased from $42 = 21 \times 2$ to $21^2 = 441$ through the proposed increasing data dimension algorithm, in which τ_α was set to be 1. The generated $\mathcal{N}_\phi - t$ curve with continuously moving windows was shown in Figure 17(a). In the figure, the red dashed lines marked the recorded anomaly time. The early

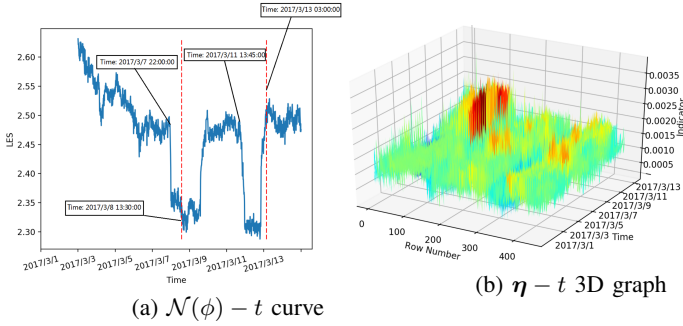


Fig. 17. Early anomaly detection and location for low-dimensional feeder.

anomaly detection process is shown as follows:

I. During 2017/3/3 00:00:00~2017/3/7 22:00:00, \mathcal{N}_ϕ decreases gradually, which indicates the operating state of the feeder is getting worse and the anomaly may occur at any time.

II. From 2017/3/7 22:00:00, \mathcal{N}_ϕ decreases dramatically, which indicates an anomaly signal occurs and the feeder operates in abnormal state. Considering the recorded anomaly time is 2017/3/8 13:30:00, it can be concluded that the anomaly is detected in an early phase. Meanwhile, it is noted that, from 2017/3/7 22:00:00 to 2017/3/9 22:00:00, the $\mathcal{N}_\phi - t$ curve is almost U-shaped and the delay lag of the anomaly signal to \mathcal{N}_ϕ is equal to the moving window's width, which coincides with the simulation result in Case 1. Similarly, from 2017/3/11 13:45:00, another new anomaly signal is detected, which is much earlier than the recorded anomaly time.

Furthermore, we located the anomalies through the proposed approach, which was shown in Figure 17(b). It can be observed that, from 2017/3/7 22:00:00, $\eta_{1\sim 63}$ increase rapidly and they are larger than others (such as η_{100}), which indicates the anomaly index set $\mathbf{I} = \{1 \sim 63\}$. For example, at 2017/3/7 22:15:00, the values of $1 - \alpha$ corresponding to $\eta_{\mathbf{I}}$ and η_{100} are 96.74% ~ 98.91% and 42.32%, respectively. Let $n = 21$, then the anomaly indexes in the original data set can be calculated by $\{\mathbf{I} \bmod n\}$, i.e., $\{1, 2, 3\}$. Similarly, from 2017/3/11 13:45:00, $\eta_{1\sim 42, 106\sim 126}$ increase rapidly and they are larger than others (such as η_{200}), which determines the anomaly index set $\mathbf{I}' = \{1 \sim 42, 106 \sim 126\}$. For example, at 2017/3/11 14:00:00, the calculated values of $1 - \alpha$ corresponding to $\eta_{\mathbf{I}'}$ and η_{200} are 99.97% ~ 99.99%, 99.99% ~ 99.99% and 38.27%, respectively. Then the anomaly indexes in the original data set can be calculated by $\{\mathbf{I}' \bmod n\}$, i.e., $\{1, 2, 7\}$. The anomaly location results coincide with the recorded anomaly indexes.

V. CONCLUSION

Based on the RMT, a data-driven approach is proposed for early anomaly detection and location in distribution networks. It is capable of detecting and locating the anomaly in an early phase by exploring the variation of the data correlation. The linear eigenvalue statistics give insight into the data behavior from a high-dimensional perspective, which serve as the anomaly detection indicator in the proposed approach. As for the low observability feeders in the distribution network, an increasing data dimension algorithm is designed for

them to be analyzed more accurately. The proposed approach is purely data-driven without requiring complex parameter information of the distribution network. It merges anomaly detection and location functionalities, and is robust against random fluctuations and measuring errors. Case studies on synthetic data corroborate the effectiveness and advantages of the proposed approach. Through real-world online monitoring data, the proposed approach is validated and it can be applied for spatio-temporal data analysis in distribution networks.

In our future work, we will focus on the application of the proposed approach for the analysis of different types of faults, including single-phase fault, two-phase fault, three-phase fault, etc. The linear eigenvalue statistics via different test functions are considered as different filters, and we can use them to track different types of fault signals.

REFERENCES

- [1] M. R. Jaafari Mousavi, "Underground distribution cable incipient fault diagnosis system," Ph.D. dissertation, 2007.
- [2] S. Sarri, L. Zanni, M. Popovic, J. Y. L. Boudec, and M. Paolone, "Performance assessment of linear state estimators using synchrophasor measurements," *IEEE Trans. Instrum. Meas.*, vol. 65, no. 3, pp. 535–548, Mar. 2016.
- [3] F. Aminifar, M. Shahidehpour, M. Fotuhi-Firuzabad, and S. Kamalinia, "Power system dynamic state estimation with synchronized phasor measurements," *IEEE Trans. Instrum. Meas.*, vol. 63, no. 2, pp. 352–363, Feb. 2014.
- [4] B. A. Alcaide-Moreno, C. R. Fuente-Esquivel, M. Glavic, and T. Van Cutsem, "Electric power network state tracking from multirate measurements," *IEEE Trans. Instrum. Meas.*, vol. 67, no. 1, pp. 33–44, Jan. 2018.
- [5] J. Ma and S. Perkins, "Time-series novelty detection using one-class support vector machines," *Proc. IJCNN*, pp. 1741–1745, 2003.
- [6] L. Xie, Y. Chen, and P. R. Kumar, "Dimensionality reduction of synchrophasor data for early event detection: Linearized analysis," *IEEE Trans. Power Syst.*, vol. 29, no. 6, pp. 2784–2794, Nov. 2014.
- [7] P. Malhotra, L. Vig, G. Shroff, and P. Agarwal, "Long short term memory networks for anomaly detection in time series," *Proc. ESANN*, pp. 89–94, 2015.
- [8] L. Chu, R. C. Qiu, X. He, Z. Ling, and Y. Liu, "Massive streaming pmu data modeling and analytics in smart grid state evaluation based on multiple high-dimensional covariance tests," *IEEE Trans. Big Data*, vol. PP, no. 99, pp. 1–1, Mar. 2016.
- [9] M. Pignati, L. Zanni, P. Romano, R. Cherkaoui, and M. Paolone, "Fault detection and faulted line identification in active distribution networks using synchrophasors-based real-time state estimation," *IEEE Trans. Power Del.*, vol. 32, no. 1, pp. 381–392, Feb. 2017.
- [10] M. Wu and L. Xie, "Online detection of low-quality synchrophasor measurements: A data-driven approach," *IEEE Trans. Power Syst.*, vol. 32, no. 4, pp. 2817–2827, Jul. 2017.
- [11] J. Liu, J. Guo, P. Orlik, M. Shibata, D. Nakahara, S. Mii, and M. Takáč, "Anomaly detection in manufacturing systems using structured neural networks," *13th WCICA*, pp. 175–180, 2018.
- [12] J. Wishart, "The generalised product moment distribution in samples from a normal multivariate population," *Biometrika*, vol. 20, no. 1/2, pp. 32–52, 1928.
- [13] R. C. Qiu, Z. Hu, H. Li, and M. C. Wicks, *Cognitive radio communication and networking: Principles and practice*. Hoboken, NJ, USA: Wiley, 2012.
- [14] N. A. S. B. K. Saad, *Random Matrix Theory with Applications in Statistics and Finance*. Canada: Ottawa, 2013.
- [15] K. Chaitanya, "Random matrix theory approach to quantum mechanics," *arXiv preprint arXiv:1501.06665*, 2015. [Online]. Available: <https://arxiv.org/pdf/1501.06665.pdf>
- [16] X. He, Q. Ai, R. C. Qiu, W. Huang, L. Piao, and H. Liu, "A big data architecture design for smart grids based on random matrix theory," *IEEE Trans. Smart Grid*, vol. 8, no. 2, pp. 674–686, Mar. 2017.
- [17] X. Xu, X. He, Q. Ai, and R. C. Qiu, "A correlation analysis method for power systems based on random matrix theory," *IEEE Trans. Smart Grid*, vol. 8, no. 4, pp. 1811–1820, Jul. 2017.

- [18] W. Liu, D. Zhang, X. Wang, D. Liu, and X. Wu, "Power system transient stability analysis based on random matrix theory," *Proc. CSEE*, vol. 36, no. 18, pp. 4854–4863, Oct. 2016.
- [19] X. Wu, D. Zhang, D. Liu, W. Liu, and C. Deng, "A method for power system steady stability situation assessment based on random matrix theory," *Proc. CSEE*, vol. 36, no. 20, pp. 5414–5420, Dec. 2016.
- [20] R. C. Qiu and M. Wicks, *Cognitive Networked Sensing and Big Data*. New York, NY, USA:Springer, 2014.
- [21] V. A. Marčenko and L. A. Pastur, "Distribution of eigenvalues for some sets of random matrices," *Sbornik: Math*, vol. 1, no. 4, pp. 457–483, 1967.
- [22] M. Shcherbina, "Central limit theorem for linear eigenvalue statistics of the wigner and sample covariance random matrices," *arXiv preprint arXiv:1101.3249*, 2011. [Online]. Available: <https://arxiv.org/pdf/1101.3249.pdf>
- [23] R. C. Qiu, *A Mathematical Introduction to Deep Learning: A Random Matrix Theory Approach*. In preprint, 2018.
- [24] A. Ambainis, A. W. Harrow, and M. B. Hastings, "Random tensor theory: Extending random matrix theory to mixtures of random product states," *Commun. Math. Phys.*, vol. 310, no. 1, pp. 25–74, 2012.
- [25] A. Lytova, "Central limit theorem for linear eigenvalue statistics for a tensor product version of sample covariance matrices," *J. Theor. Prob.*, pp. 1–34, 2017.
- [26] R. D. Zimmerman, C. E. Murillo-Sanchez, and R. J. Thomas, "Matpower: Steady-state operations, planning, and analysis tools for power systems research and education," *IEEE Trans. Power Syst.*, vol. 26, no. 1, pp. 12–19, Feb. 2011.
- [27] R. D. Zimmerman and C. E. Murillo-Sánchez, "Matpower 6.0 users manual," Dec. 2016.